Temperature-dependent band gap, interband transitions, and exciton formation in transparent *p*-type delafossite $CuCr_{1-x}Mg_xO_2$ films

Xurui Li (李旭瑞), Meijie Han (韩美杰), Xiaolong Zhang (张小龙), Chao Shan (单超), Zhigao Hu (胡志高),* Ziqiang Zhu (朱自强), and Junhao Chu (褚君浩)

Key Laboratory of Polar Materials and Devices, Ministry of Education, Department of Electronic Engineering, East China Normal University, Shanghai 200241, China

(Received 24 March 2014; revised manuscript received 2 June 2014; published 14 July 2014)

Temperature-dependent interband transitions and exciton excitations of sol-gel derived $CuCr_{1-x}Mg_xO_2$ ($2\% \leqslant x \leqslant 8\%$) films have been investigated by transmittance spectra (8–300 K) and photoluminescence (PL) spectra (77–300 K). An abnormal dependence of the optical band gap with the temperature has been found for the films with $x = 0.02$ and 0.04. At the low-temperature region, the gap energy shows a redshift trend with decreasing temperature. It is due to the strong Cr 3*d*-O 2*p*-Cu 3*d* interaction in the upper part of the valence band, which can be weaken by heavily Mg doping. The spin-orbit interactions of Cr^{3+} ions in an octahedral environment make the 3*d* states more disperse, which can contribute to the relatively high conductivity. A well-defined low-energy absorption has been assigned to the spin-allowed $3d \rightarrow 3d$ transition. Moreover, a strong exciton excitation around 1.8 eV has been observed due to the naturally low-dimensional structure of the delafossite, which can be modulated by temperature and hole concentration.

DOI: 10.1103/PhysRevB.90.035308 PACS number(s): 68.55.Ln, 78.20.−e, 78.55.−m

I. INTRODUCTION

Transparent conducting oxides (TCOs) are promising candidate materials with wide applications from solar cells to field effect transistors (FETs) [1,2]. The TCOs are assigned to be used in the fabrication of functional *p*-*n* junctions, which is the basic constituent for a variety of transparent electronic devices. Generally, TCO requires the material to be as transparent as a glass, while its conductivity approaches the metallic behavior. Unfortunately, a higher resistivity and lower transparency make *p*-type TCOs more elusive in contrast with traditional *n*-type TCOs, such as ZnO, In_2O_3, and SnO_2 [3]. The main reason is that the top of the valence band is predominately composed of oxygen (O) 2*p* states in classical TCOs. The valence-band edge of TCOs is strongly localized on O ions because of the large electronegativity of oxygen [4]. It is difficult to introduce positive holes into these bands because oxidizing oxygen is not easy in chemical terminology.

One way to reduce the localization of the valence-band edge is to introduce cations with closed-shell levels [5]. Metals with complete low-binding-energy *d* shells, such as Cu and Ag, can help to push up a more disperse band state by the coupling between 2*p* levels of O ions and the closed-shell valence electronic configurations [6]. Moreover, the closed *d* shell can impede the $d \rightarrow d$ transitions that could absorb light in the visible range. For example, the upper valence band states in Cu_2O are of dominant Cu 3*d* atomic character. The introduction of holes involving oxidation of $3d^{10}$ Cu(I) to $3d^9$ Cu(II) indicates a *p*-type semiconductor character. However, the electronic gap of Cu_2O is on the order of 2 eV, which is much lower than what is needed for application in TCO devices. The fact that a large Cu 3*d* bandwidth arises from strong Cu-Cu interaction should account for the relatively small band gap of Cu_2O [7]. Recently, the delafossite-structured $CuMO_2$ (*M*=Al, Ga, Cr, etc.) oxides have attracted much more attention as potential candidates for *p*-type TCOs, due to the pioneering work on the transparent $CuAlO_2$ conductive film in Refs. [5,8]. Interesting optical and electronic properties have been found due to the reduced dimensionality of next-nearest-neighbor Cu-Cu interactions in these materials.

Among $CuMO_2$ systems, it was found that $CuCrO_2$ has a conductivity of the order of 1 S cm^{-1}. Upon doping with 5% Mg, the conductivity can be increased to 220 S cm^{-1}, which is the highest among delafossite-structured ABO_2 compounds. It shows a potential candidate for fabricating optoelectronic devices [9]. In our previous work, the sol-gel derived $CuCr_{1-x}Mg_xO_2$ films have been proved to possess relatively high transmittance above 70% in the visible-near-infrared wavelength region. It has been found that the conductivity of $CuCr_{1-x}Mg_xO_2$ increases with the temperature from 150 to 300 K. There is a transition of the carrier transport mechanism from a thermal activation behavior to a variable range hopping at a certain temperature [3,10]. Nevertheless, the origins of absorption behavior and electrical transport properties have not been clarified to date. Generally, the optical and electrical behaviors are directly affected by electronic band structure. Although theoretical researches have been carried out to study the band structure of $CuCr_{1-x}Mg_xO_2$, few studies about the temperature and doping dependence of the electronic structure for the $CuCr_{1-x}Mg_xO_2$ system have been performed [11,12]. By investigating these controllable influences on the optical response, one can understand the electronic band structure and develop energy band engineering for $CuCr_{1-x}Mg_xO_2$-based TCO devices.

In this paper, transmittance and photoluminescence (PL) spectra of $CuCr_{1-x}Mg_xO_2$ ($2\% \leqslant x \leqslant 8\%$) films have been measured in the temperature regions of 8–300 K and 77–300 K, respectively. By assigning the absorption and excitation peaks, the electronic band structure of $CuCr_{1-x}Mg_xO_2$ has been

*zghu@ee.ecnu.edu.cn

 ©2014 American Physical Society

discussed in detail. The electronic band structure scenario can explain the spectral and electrical behavior for $CuCr_{1-x}Mg_xO_2$ films well.

II. EXPERIMENTAL DETAILS

The $CuCr_{1-x}Mg_xO_2$ films were prepared on (001) sapphire substrates by the sol-gel route employing a spin-coating process. The deposited films were preheated at 300 °C for 5 min in air by a rapid thermal processing. The above process (spin-coating and preheating) was repeated several times in order to obtain films with the desired thickness. Finally, the films were annealed at 700 °C for 30 min in N_2 with a flow of 2.5 L/min. The crystalline structure of the $CuCr_{1-x}Mg_xO_2$ films was investigated by x-ray diffraction (XRD) technique. It can be seen that all the films are polycrystalline with a stronger (006) diffraction peak (not shown). The results indicate that the films with Mg doping are preferentially oriented along the c axis perpendicular to the substrate surface. A detailed fabrication procedure and the film structure parameters can be found in Ref. [10].

The normal-incident transmittance spectra were measured by a double beam ultraviolet-infrared spectrophotometer (PerkinElmer UV/VIS Lambda 950) at the photon energy of 2650–190 nm (0.5–6.5 eV) with an interval of 2 nm. The samples were mounted on a cold stage of an optical cryostat (Janis SHI-4-1) and capable of cooling from 300 to 8 K [13]. Photoluminescence (PL) spectra were carried out by a Jobin-Yvon LabRAM HR 800 UV spectrometer with an Ar^+ laser as the exciting source, which is operated at the wavelength of 488 nm. The PL data were recorded from 77 to 300 K using a Linkam THMSE 600 heating/cooling stage with the set-point stability of better than 1 K. The laser beam was focused through a 50× microscope with a working distance of 18 mm. An air-cooled charge coupled device (CCD) (−70 °C) with a 1024×256 pixels front illuminated chip was used to collect the luminescence signal dispersed on 1800 grooves/mm grating. Note that no mathematical smoothing has been performed on the experimental data.

III. RESULTS AND DISCUSSION

A. Temperature-dependent transmittance

Transmittance spectra for all films at room temperature have been shown in Fig. 1(a). It can be found that the films are transparent, with relatively high optical transmittance above 70% in the visible range. Transmittance spectra of $CuCr_{0.98}Mg_{0.02}O_2$ film at different temperatures are plotted in Fig. 1(b). Obviously, the spectra at a higher temperature present a weaker shoulder structure. An enlarged spectral region for the film with $x = 0.02$ and 0.08 near the absorption edge is shown in Figs. 1(c) and 1(d), respectively. As can be seen, the absorption edge for the film with $x = 0.08$ shows a blueshift trend with decreasing temperature. However, a nonmonotonic trend has been found for the films $x = 0.02$ and 0.04 (not shown), with the absorption edge showing a redshift trend with decreasing temperature at low temperatures. To study the band-gap behavior in detail, a three-phase layered structure (air/film/substrate) is applied to simulate the transmittance spectra of the $CuCr_{1-x}Mg_xO_2$ films. As we know, the imaginary part ε_2 of the complex dielectric function can usually be expressed by the Tauc-Lorentz (TL) model [14]:

$$\varepsilon_2 = \frac{AE_o\Gamma(E-E_n)^2}{\left[\left(E^2-E_o^2\right)^2+\Gamma^2E^2\right]^2}\frac{1}{E}, \quad E > E_n,$$
$$\varepsilon_2 = 0, \quad E < E_n. \tag{1}$$

Here, E_o is the peak transition energy, E_n is the excitation gap energy, Γ is the broadening parameter, and A is the factor which represents the optical transition matrix elements. The real part ε_1 of the complex dielectric function is obtained by the Kramers-Krönig integral of ε_2:

$$\varepsilon_1 = \varepsilon_\infty + \frac{2}{\pi}P\int_{E_n}^{\infty}\frac{\xi\varepsilon_2(\xi)}{\xi^2-E^2}d\xi. \tag{2}$$

Here, ε_∞ represents the contribution of the optical transitions at higher energies and appears as an additional fitting parameter. The multiple TL model, which is the sum of several single-TL terms, generally corresponds to the multitransitions. Three TL oscillator functions here were used to express the optical response of the $CuCr_{1-x}Mg_xO_2$ films well [15]. For instance, the TL parameter values of the $CuCr_{1-x}Mg_xO_2$ films at 8, 120, 220, and 300 K are listed in Table II (see Appendix). A good agreement between the experimental and calculated spectra can be found over the entire phonon energy region, as plotted by the solid lines in Figs. 1(a) and 1(b).

The optical band-gap energy can be estimated by an intercept of the $(\alpha h\nu)^n$ plot with the photon energy $h\nu$ [16]. The absorption coefficient α for the film can be determined from the transmittance (Tran): $\alpha = -\ln(\text{Tran})/d$, where d is the layer thickness. The relationship between the absorption coefficient and the incident photon energy can be written in the Tauc's relation as

$$(\alpha h\nu)^n = C(h\nu - E_{\text{OBG}}). \tag{3}$$

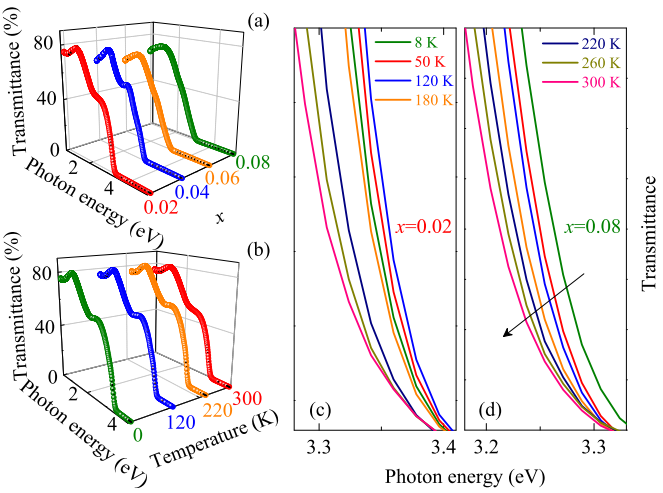

FIG. 1. (Color online) (a) Transmittance spectra for the $CuCr_{1-x}Mg_xO_2$ films at room temperature. (b) Transmittance spectra for $CuCr_{0.98}Mg_{0.02}O_2$ at the temperatures of 8, 120, 220, and 300 K. (c) An enlarged spectral region for the films with $x = 0.02$ and 0.08 near the absorption edge at different temperatures.

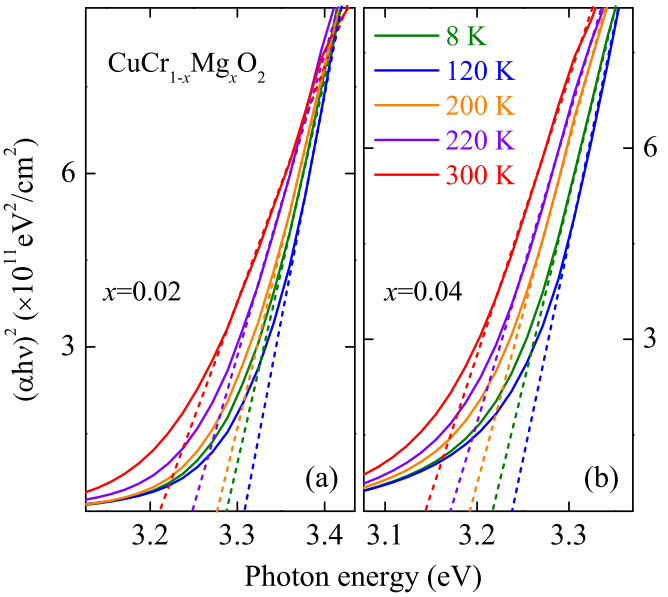

FIG. 2. (Color online) Plot of $(\alpha h\nu)^2$ vs the photon energy for the determinations of direct optical band-gap energies for the (a) $CuCr_{0.98}Mg_{0.02}O_2$ and (b) $CuCr_{0.96}Mg_{0.04}O_2$ films.

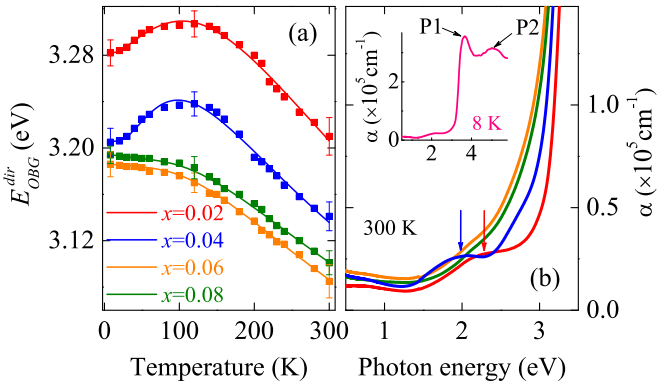

FIG. 3. (Color online) (a) Temperature-dependent E_{OBG}^{dir} for the $CuCr_{1-x}Mg_xO_2$ films are plotted with the best-fitting lines. (b) Absorption spectra for all $CuCr_{1-x}Mg_xO_2$ films at room temperature. The inset shows the absorption spectra for the $CuCr_{0.98}Mg_{0.02}O_2$ film at 8 K.

Here, C is a constant and E_{OBG} is the optical band gap. The exponent n depends on the type of transition, where n is 2 for direct band gap (E_{OBG}^{dir}) and 1/2 for indirect band gap (E_{OBG}^{indir}) transitions, respectively. For example, from Fig. 2, the E_{OBG}^{dir} can be estimated to be 3.22 eV at 300 K and 3.29 eV at 8 K for the film with $x = 0.02$, while for the film with $x = 0.04$ it is 3.14 and 3.21 eV, respectively. The results are in good agreement with the parameter E_o of oscillator TL_1 at the corresponding temperature, indicating that the TL_1 oscillator is associated with a direct band gap. Note that the band-gap values coincide with the previous reports [17]. It has been proved that there is a E_{OBG}^{dir} of about 3.25 eV at the F point for $CuCrO_2$ using the screened-exchange local density approximation (sX-LDA) hybrid functional [18]. Thus the transtion E_o of TL_1 can be assigned to the E_{OBG}^{dir} at the F point.

B. Band-gap variation with the temperature

Temperature dependence of the E_{OBG}^{dir} for the $CuCr_{1-x}Mg_xO_2$ films from the best-fitting parameters E_{o1} are shown in Fig. 3(a). Unlike other two films, the band-gap energy of $CuCr_{0.98}Mg_{0.02}O_2$ and $CuCr_{0.96}Mg_{0.04}O_2$ films shows a nonmonotonic trend with decreasing temperature. The minimum band-gap energy appears at the highest temperature of 300 K. However, the maximum energy for the films with $x = 0.02$ and 0.04 appears at about 120 K, instead of the lowest temperature 8 K. Recently, some binary and ternary compounds with monovalent Cu or Ag cation, such as CuCl, $CuGaS_2$, and $AgGaSe_2$, have been proved to possess anomalous temperature behavior. There is a maximum gap energy at a relatively low temperature T_m, below which the gap energy decreases with the temperature, or extends as a flat plateau [19–21]. The band-gap shrinkage with the temperature above T_m is usually attributed to the electron-phonon interaction and the lattice thermal expansion. On the other hand, it suggests that the anomalous behavior in low temperature region is related to p-d electron hybridization between d-like valence electrons (e.g., Cu 3d or Ag 4d) and p-like counterparts (e.g., O 2p or Se 4p). Although it was previously found that the nonmonotonic behavior is indeed present for Cu compounds like $CuGaS_2$, it is usually much weaker than that in the Ag compounds. The difference is ascribed to different degree of p-d hybridization at the top of valence band, which is modulated by the electron-optical-phonon interaction [19,21]. The Cu 3d energy level is somehow separated from the occupied p levels, as compared to the Ag 4d energy level. Nevertheless, it has been confirmed for $CuCr_{1-x}Mg_xO_2$ that there also exists certain degree of Cr 3d-O 2p-Cu 3d hybridization in the upper part of the valence band [12]. Namely, the occupied Cr 3d states interact covalently with the neighboring O states. It enhances the p-d hybridization and makes the nonmonotonic behavior clearer for the present $CuCr_{1-x}Mg_xO_2$ system.

Usually, the Urbach tail can be used to get useful information about the structural disorder in semiconductors, as well as the electron-phonon interactions and electric-field-induced ionization of the excitons [22,23]. The absorption coefficient just below the fundamental absorption edge can be expressed by the Urbach's rule:

$$\alpha = \alpha_0 \exp[\sigma(h\nu - E_0)/k_B T], \quad (4)$$

where α_0 and E_0 are characteristic parameters of the material, σ is the steepness parameter, and k_B is the Boltzmann constant. The relation $k_B T/\sigma$ is called as Urbach energy (E_U), which represents the width of the exponential tail. For clarity, the plot of $\ln\alpha$ versus photon energy for the $CuCr_{1-x}Mg_xO_2$ films at room temperature is shown in Fig. 4. The parameter E_U can be obtained from the reciprocal of the slope in the linear part. It can also be found that the Urbach tail appears for all films. As can be seen in the inset of Fig. 4, the Urbach energy E_U gradually increases with the temperature. In the case of Urbach tail, the thermal dissociation effect may lead to the anomalous temperature variation of the band gap.

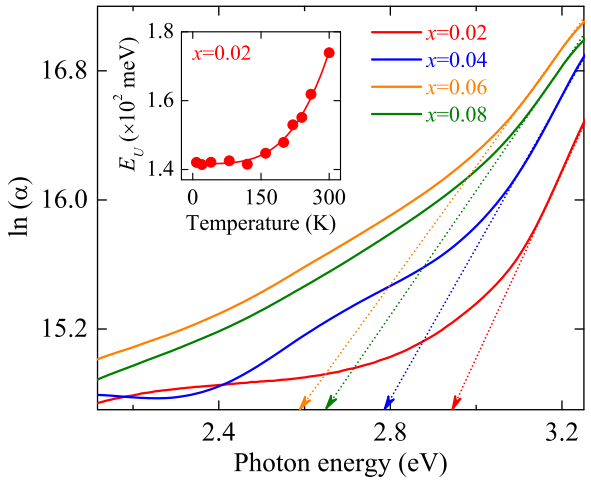

FIG. 4. (Color online) The Urbach energy E_U determined from lnα vs photon energy at room temperature. Note that the inset shows temperature dependence of E_U for the $CuCr_{0.98}Mg_{0.02}O_2$ film.

However, the $CuCr_{1-x}Mg_xO_2$ films with heavily Mg doping have a larger value of E_U. It represents more extensive area influenced by the Urbach tail. Nevertheless, the anomalous temperature variation cannot be observed for the films with increasing Mg doping, indicating the complex effect on the *p-d* hybridization from electron-optical-phonon interaction. With increasing Mg doping composition, more Cr sites and even Cu can be substituted. Therefore stronger disturbance of the local spin fluctuation at Cr sites can appear and much weaker *p-d* hybridization drives the heavily doped $CuCr_{1-x}Mg_xO_2$ system into the normal state.

The nonmonotonic behavior from both lattice dilation and electron-phonon interaction can be represented by lattice vibrations, which corresponds to more than one Bose-Einstein oscillators [19]. Recently, it has been manifested that a modified model including extra low-energy Bose-Einstein oscillators can account well for the nonmonotonic temperature dependence of the gaps:

$$E(T) = E_0 + \sum_{i=1}^{2} N_i[2n_{BE}(\Theta_i/T) + 1]. \quad (5)$$

Here, N_i is the weight which, if negative, describes the degree of the energy increase with decreasing temperature; the Einstein characteristic temperature Θ_i is defined as E_i/k_BT, where E_i is the energy for oscillator. The parameter n_{BE} is the Bose-Einstein factor:

$$n_{BE}(\Theta_i/T) = 1/[\exp(\Theta_i/T) - 1]. \quad (6)$$

Two oscillators were applied for fitting the temperature dependence of the gaps. The best-fitting parameters are summarized in Table I. As can be seen, for the two films ($x = 0.02$ and 0.04) with nonmonotonic behavior, the low-energy weight N_2 has a positive sign. The first normal oscillator results in the increase of the gap with decreasing temperature, while in the low-temperature region, the oscillator with opposite weight makes a greater contribution and leads to the decline. For the other two compositions, the parameter N_2 has the same sign with the first normal weight N_1, indicating that the low-energy oscillator also makes contribution to the increase of the gap with decreasing temperature.

C. Electronic band structure

To explore the electronic structure of $CuCr_{1-x}Mg_xO_2$ films in detail, the absorption spectra for $CuCr_{1-x}Mg_xO_2$ films are necessary. The inset of Fig. 3(b) shows the absorption spectra for $CuCr_{0.98}Mg_{0.02}O_2$ in the energy region between 0.5 and 5.8 eV at 8 K. The absorption onset energy is found to be around 3.2 eV. The fundamental absorption edge indicates that there should be a strong excitation, corresponding to the direct transition from valence-band maximum (VBM) to the conduction-band minimum (CBM) [24]. A well-defined absorption maximum at about 3.65 eV can be found, which agrees with the previous reports [25,26]. This is attributed to the dipole-allowed Cu $3d$ + O $2p \rightarrow$ Cu $3d_{z^2} + 4s$ transition, which is dipole forbidden for Cu_2O. Another peak centered around 5 eV can also be found. The theoretical work suggests that the $3d^3$ Cr^{3+} ion in an octahedral environment contains a t_{2g}^3 configuration with a ground state $^4A_{2g}$ [7,25]. The ground state of free ion energy ^{4}F (identified by group theory lables) splits into three energy levels in an octahedral crystal field: the $^4A_{2g}$ ground level and two excited levels, $^4T_{2g}$ and $^4T_{1g}$. Nevertheless, the spin-allowed but dipole forbidden transition energy is relatively low (below 2.6 eV). Another higher $^4T_{1g}$ state exists, corresponding to the ^{4}P free ion state with the $^4A_{2g} \rightarrow {}^4T_{1g}(^4\text{P})$ energy located in the ultraviolet range [27]. Thus the peak centered around 5 eV can be attributed to the Cr-related charge-transfer transition of Cu $3d$ + O $2p \rightarrow$ unoccupied $^4T_{1g}(^4\text{P})$. The center of the empty $^4T_{1g}(^4\text{P})$ level is energetically above the Cu $3d_{z^2} + 4s$ orbitals. The layered structure for $CuCrO_2$ can be treated as a natural superlattice composed of Cu-O-Cu dumbbells and the wide band-gap insulator Cr_2O_3. The native low-dimensionality of

TABLE I. Parameters obtained from the best fit to the experimental data in Fig. 3(a) with two Bose-Einstein oscillators Θ_i (i = 1,2). The 90% confidence limits are given in parentheses.

x	E_0 (eV)	N_1 (eV)	Θ_1 (eV)	N_2 (eV)	Θ_2 (eV)
0.02	3.409 (0.019)	−0.138 (0.017)	536 (23)	0.012 (0.002)	72 (8)
0.04	3.283 (0.009)	−0.106 (0.007)	348 (28)	0.030 (0.002)	111 (12)
0.06	3.264 (0.018)	−0.077 (0.006)	459 (23)	−0.002 (0.001)	96 (10)
0.08	3.272 (0.019)	−0.076 (0.033)	477 (22)	−0.002 (0.001)	62 (8)

the delafossite structure leads to the van Hove singularities in the density of states for both valence and conduction bands, resulting in the relatively well-defined absorption peaks.

Another obvious shoulder centered just above about 2 eV can be also observed. The appearance of this shoulder indicates an additional transition for $CuCr_{1-x}Mg_xO_2$, corresponding to the best-fitting TL_2 oscillator energy value. As previously stated, two dominating hypotheses have been presented to interpret the origin of the low-energy absorption: (1) the shoulder is associated with Cu^{2+} defect states arising from cation vacancies; (2) it is ascribed to the excitation of $3d \rightarrow 3d$ transitions as a result of the covalent interaction between Cr $3d$ and O $2p$ orbitals [7,25]. To clarify the issue, the absorption spectra for all four films at room temperature are plotted in Fig. 3(b). As can be seen, the corresponding shoulder can be found only for $x = 0.02$ and 0.04, while it disappears for the other two films. It has been recently revealed that the near-Fermi-level (around the VBM) structure has both Cu $3d$ and Cr $3d$ characters [12,28]. With increasing Mg doping, Cu^{2+} defect states increase as a consequence of that more holes are introduced into the upper part of the valence band. Nevertheless, the shoulder structure vanishes with increasing Mg doping, indicating that the pattern observed here has little association with the Cu^{2+} defect states. On the other hand, there is a competition between the Cu-O bonds and Cr-O covalency [7]. With the oxidation of the Cu^{+} into Cu^{2+}, stronger bonds between Cu and O are formed, resulting in the weakness of the covalent interaction between Cr and O. The weaker excitation of $3d \rightarrow 3d$ transitions can lead to the disappearance of the shoulder structure.

As mentioned above, $CuCr_{1-x}Mg_xO_2$ with Cr^{3+} in an octahedral environment contains two low lying spin-allowed (but dipole forbidden) excitations derived from the $^4T_{2g}$ and $^4T_{1g}$ states of the excited $t_{2g}^2 e_g^1$ configuration. The low energy around 2 eV has been assigned to the allowed $^4A_{2g} \rightarrow {}^4T_{1g}(^4\mathrm{F})$ excitation using the resonant inelastic x-ray scattering (RIXS) method [7,27]. The corresponding energy of this excitation in Cr_2O_3 is 2.6 eV, which has already been confirmed [29]. The lower value for $CuCr_{1-x}Mg_xO_2$ results from the reduced Cr-O covalency due to the formation of short and strong Cu-O bonds, which is consistent with the above discussion [7,25]. The phenomenon has also confirmed the existence of the complex hybridization of the Cu-O-Cr states. Moreover, the center of the shoulder for $CuCr_{0.96}Mg_{0.04}O_2$ shifts from 2.2 to 2 eV, as compared to the results from $CuCr_{0.98}Mg_{0.02}O_2$. The multiple-electron energy-level structure for transition-metal ions with the $3d^n$ configuration is determined by the strength of the octahedral crystal field and the interelectron interaction. This is normally done through the well-known Tanabe-Sugano diagram [27,30]. The spin-split energy level is plotted against the magnitude of the octahedral crystal field with the configuration of splitting parameters for a $3d^n$ ion. The $^4A_{2g}$ and $^4T_{1g}$ levels have a large slope in the Tanabe-Sugano diagram, which means that the energy separation between these levels is dependent on the crystal field strength. With increasing Mg doping, the crystal field strength increases and the energy gap between $^4A_{2g}$ and $^4T_{1g}$ levels decreases, resulting in the redshift trend of the low-energy peak. Therefore an electronic band diagram for the $CuCr_{1-x}Mg_xO_2$ films can be proposed, as shown in Fig. 5. Here, both Cu $3d_{z^2}$ and $4s$ orbitals contribute to the CBM due to the hybridization effect. The theory that the upper part of the valence band has primarily the Cr $3d$ character can be well confirmed [12]. In fact, it has been suggested that the Mg-doped Cr_2O_3 could also be a p-type TCO with considerable wide band gap above 3 eV [31,32]. It indicates that the VBM of the present $CuCr_{1-x}Mg_xO_2$ films may be more like Cr_2O_3 than $CuAlO_2$.

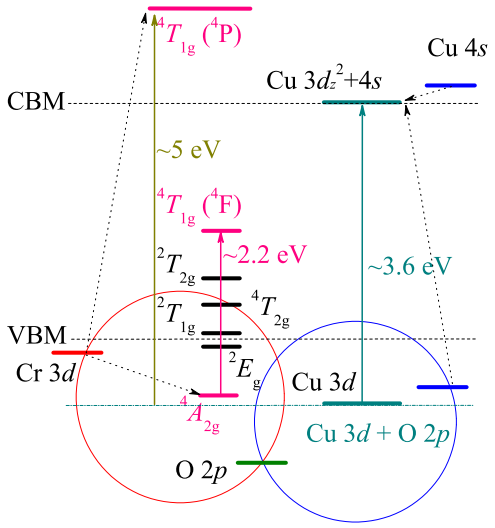

FIG. 5. (Color online) Electronic band diagram for the $CuCr_{1-x}Mg_xO_2$ films was applied to explain the experimental results.

D. Photoluminescence emissions

To explore the interband excitations in addition to the observed absorption peaks, temperature-dependent photoluminescence spectra have been studied in the temperature range of 77–300 K. As can be seen in Fig. 6(b), a well-defined shoulder around 2.2 eV is observed, corresponding to the low-energy absorption peak. As a matter of fact, a peak around 488 nm has been observed from the PL spectra for Cr_2O_3, which corresponds to the excitation energy around 2.6 eV in Cr_2O_3 [33]. It further proves that the electronic structure around VBM of $CuCr_{1-x}Mg_xO_2$ is more like Cr_2O_3 than $CuAlO_2$, as previously discussed. Meanwhile, two narrow but quite strong peaks can be found. The strongest peak centered around 1.808 eV exhibits a full width at half maximum (FWHM) of about 1 meV. The exciton emission is shifted to lower energy with increasing temperature due to the conventional lattice thermal dilation. All these characteristics manifest this peak to be neutral-donor-bound-exciton (D_0X) emission [34]. Thus the peak centered around 1.808 eV (at 8 K) can be assigned to be D_0X [Cu(I)] emission. The mixture phase of the Cu(I) and Cu(II) should account for two separate peaks. The excited state of the exciton bound to the ionized donor (Cu(II)) lies above that of the D_0X [35]. Therefore the peak centered around 1.804 eV (at 8 K) is assigned to

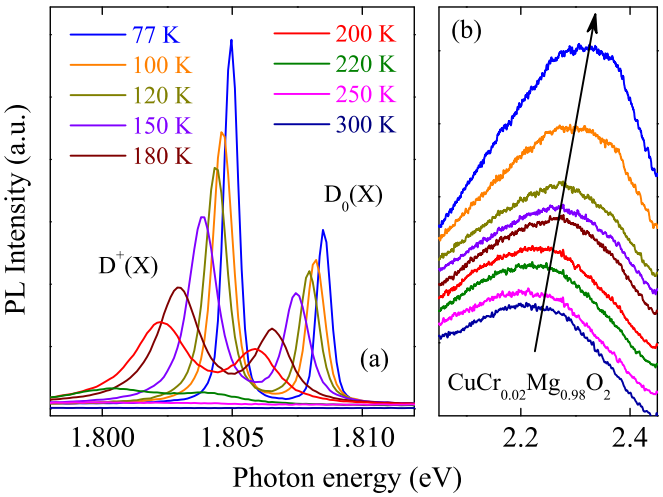

FIG. 6. (Color online) (a) Photoluminescence spectra for the $CuCr_{0.02}Mg_{0.98}O_2$ film in the energy region from 1.798 eV to 1.812 eV at different temperatures. (b) Emission spectra in an enlarged energy region from 2.05 eV to 2.45 eV at different temperatures.

the ionized-donor-bound-exciton D^+X [Cu(II)] emission. The relatively weaker PL intensity for D_0X [Cu(I)] emission is due to the heavier effective mass, as compared to that of Cu(II) state. The free exciton (FX) peak deduced from the D_0X peak should be above 1.8 eV. The D_0X emission has a typical Cu(I) characteristic. It indicates that the exciton binding energy is similar to Cu_2O, which has previously been estimated to be about 140 meV [36]. Thus the latent FX exciton peak center can be estimated to be around 1.948 (1.808+0.14) eV, which can be overlapped by the broadening peak of the Cr $3d \rightarrow 3d$ excitation around 2 eV [36,37]. Furthermore, the bound-exciton emission is quenched at temperatures above 220 K, indicating that the narrow lines are not related to deep levels. In spite of the high exciton binding energy, reports on room-temperature exciton observations for Cu_2O and $CuCrO_2$ systems are quite limited. The exciton-related signal vanishing above 220 K can be explained in terms of a bound state of exciton coupled primarily to Cu vacancy [38].

It has been manifested that there is a transition of carrier transport mechanism from a thermal activation behavior to a variable range hopping (VRH) at a special temperature T_{cross} [3,39]. The VRH mechanism has also been observed in Cr_2O_3, indicating the similarity between the band structure around VBM from $CuCr_{1-x}Mg_xO_2$ and Cr_2O_3 [40]. Hopping transport requires the existence of localized states around the Fermi level [41,42]. In the temperature region below T_{cross}, the decrease of the thermal energy depresses the hopping between the nearest-neighbor Cu sites. Hops over longer distance but with closer energy spacing are more favorable, changing the transport mechanism into the Mott VRH [43]. The contributions from the hopping to Cr sites and Cu sites in the other layers (but with closer energy) become relatively dominant. Thus the conductivity shows a three-dimensional VRH behavior [39]. The peak intensity is nearly quenched out at about 220 K, which is in accord with the T_{cross} [3]. It indicates that the localization for the exciton excitation shares the same origin of the localized states for VRH. In addition, it can also explain why the excitation from the Cu 3*d*-O 2*p* hybridization states to Cr 3*d* states (with the absorption peak centered around 5 eV) is allowed in the low-temperature region.

There is a troublesome issue that the increasing rate of the conductivity for $CuCr_{1-x}Mg_xO_2$ films gradually slows down and reaches a maximum at about $x = 0.06$, which can be generally explained by the less effective substitution. More important reason is that the overdoping Mg disturbs the up-spin Cr 3*d* orbitals, which greatly impedes the dispersion of the 3*d* states [10]. The less disperse electronic states decrease the effective transport and holds back the increase of the conductivity. As the transport mechanism changes from a thermal activation behavior to a variable range hopping one, the contributions from the hopping to Cr sites become dominant. The increase of the hole density around Cr sites enhances the probability of the spin-allowed excitation and increases the intensity of the Cr $3d \rightarrow 3d$ peak. The strength of the octahedral crystal field also increases with decreasing temperature. It elevates the energy gaps between the Cr excited states and ground states, which induces the blueshift for the low-energy shoulder peaks with decreasing temperature. The more disperse Cr 3*d* states elevate the VBM, making contribution to the redshift trend of optical band gap at low temperatures.

IV. SUMMARY

In summary, interband transitions and exciton excitations of sol-gel derived $CuCr_{1-x}Mg_xO_2$ films with different Mg doping composition have been investigated by temperature-dependent transmittance and photoluminescence spectra. It has been proved that the upper part of the valence band has primarily the Cr 3*d* character with a minor contribution from the Cu 3*d*. The well-defined low-energy absorption peak has been assigned to the Cr^{3+} $^4A_{2g} \rightarrow {}^4T_{1g}(^4F)$ excitation. The abnormal redshift optical band gap with decreasing temperature in the low temperature region is due to the Cr 3*d*-O 2*p*-Cu 3*d* interaction. The overdoping Mg disturbs the up-spin Cr 3*d* orbitals and increases the density of Cu^{2+} defects, which drives the temperature-dependent band-gap behavior into the normal states. Moreover, the disturbance greatly impedes the effective transport and holds back the conductivity increment.

ACKNOWLEDGMENTS

One of the authors (X.R.L.) is grateful to Kai Jiang for the technical supports. This work was financially supported by Major State Basic Research Development Program of China (Grant Nos. 2011CB922200 and 2013CB922300), Natural and Science Foundation of China (Grant Nos. 11374097 and 61376129), Projects of Science and Technology Commission of Shanghai Municipality (Grant Nos. 14XD1401500, 13JC1402100 and 13JC1404200), and the Program for Professor of Special Appointment (Eastern Scholar) at Shanghai Institutions of Higher Learning.

APPENDIX

TABLE II. The Tauc-Lorentz oscillator parameter values at different temperatures (8, 120, 220, and 300 K) for $CuCr_{0.98}Mg_{0.02}O_2$ and room-temperature values for other three films are taken from the best fit to transmittance spectra. The 90% confidence limits are given in parentheses.

x	T (K)	ε_∞	TL_j	A_j (eV)	E_{oj} (eV)	Γ_j (eV)	E_{nj} (eV)
0.02	8	3.11	$j=1$	118 (4)	3.28 (0.01)	1.95 (0.05)	2.93 (0.08)
		(0.02)	$j=2$	18.3 (0.1)	2.32 (0.04)	1.92 (0.02)	2.08 (0.06)
			$j=3$	5.06 (0.11)	1.29 (0.02)	1.72 (0.04)	0.95 (0.05)
	120	3.12	$j=1$	120 (2)	3.30 (0.01)	1.94 (0.07)	2.95 (0.05)
		(0.03)	$j=2$	18.3 (0.1)	2.29 (0.04)	1.92 (0.05)	2.07 (0.07)
			$j=3$	5.13 (0.07)	1.29 (0.05)	1.68 (0.12)	0.94 (0.02)
	220	3.12	$j=1$	124 (4)	3.25 (0.01)	1.90 (0.06)	2.89 (0.06)
		(0.03)	$j=2$	18.1 (0.2)	2.23 (0.08)	1.99 (0.05)	2.01 (0.04)
			$j=3$	5.13 (0.07)	1.27 (0.02)	1.87 (0.14)	0.88 (0.04)
	300	3.14	$j=1$	125 (2)	3.21 (0.02)	1.89 (0.06)	2.87 (0.09)
		(0.02)	$j=2$	18.1 (0.2)	2.21 (0.02)	2.13 (0.05)	1.92 (0.03)
			$j=3$	4.96 (0.05)	1.26 (0.03)	1.86 (0.07)	0.86 (0.04)
0.04	300	3.18	$j=1$	125 (4)	3.14 (0.01)	1.85 (0.05)	2.84 (0.04)
		(0.09)	$j=2$	18.1 (0.2)	2.08 (0.03)	2.37 (0.11)	1.82 (0.03)
			$j=3$	4.72 (0.06)	1.21 (0.04)	1.72 (0.13)	0.81 (0.05)
0.06	300	3.19	$j=1$	129 (5)	3.09 (0.02)	1.97 (0.04)	2.72 (0.07)
		(0.05)	$j=2$	2.23 (0.12)	2.05 (0.07)	0.81 (0.02)	1.80 (0.03)
			$j=3$	2.08 (0.09)	1.13 (0.03)	1.70 (0.03)	0.81 (0.02)
0.08	300	3.17	$j=1$	127 (4)	3.10 (0.01)	1.82 (0.02)	2.88 (0.04)
		(0.04)	$j=2$	1.26 (0.13)	2.06 (0.08)	1.03 (0.04)	1.82 (0.05)
			$j=3$	1.61 (0.09)	1.09 (0.12)	1.01 (0.03)	0.72 (0.02)

[1] T. Minami, Semicond. Sci. Technol. **20**, S35 (2005).

[2] S. Dasgupta, S. Gottschalk, R. Kruk, and H. Hahn, Nanotechnol. **19**, 435203 (2008).

[3] X. R. Li, M. J. Han, P. Chang, Z. G. Hu, Y. W. Li, Z. Q. Zhu, and J. H. Chu, Appl. Phys. Lett. **104**, 012103 (2014).

[4] A. Kudo, H. Yanagi, H. Hosono, and H. Kawazoe, Appl. Phys. Lett. **73**, 220 (1998).

[5] H. Kawazoe, M. Yasukawa, H. Hyodo, M. Kurita, H. Yanagi, and H. Hosono, Nature (London) **389**, 939 (1997).

[6] S. Sheng, G. J. Fang, C. Li, S. Xu, and X. Z. Zhao, Phys. Stat. Sol. (a) **203**, 1891 (2006).

[7] T. Arnold, D.J. Payne, A. Bourlange, J.P. Hu, R.G. Egdell, L.F.J. Piper, L. Colakerol, A. DeMasi, P.A. Glans, T. Learmonth, K.E. Smith, J. Guo, D.O. Scanlon, A. Walsh, B.J. Morgan, and G.W. Watson, Phys. Rev. B **79**, 075102 (2009).

[8] M. J. Han, K. Jiang, J. Z. Zhang, W. L. Yu, Y. W. Li, Z. G. Hu, and J. H. Chu, J. Mater. Chem. **22**, 18463 (2012).

[9] R. Nagarajan, A. D. Draeseke, A. W. Sleight, and J. Tate, J. Appl. Phys. **89**, 8022 (2001).

[10] M. J. Han, Z. H. Duan, J. Z. Zhang, S. Zhang, Y. W. Li, Z. G. Hu, and J. H. Chu, J. Appl. Phys. **114**, 163526 (2013).

[11] D. O. Scanlon and G. W. Watson, J. Mater. Chem. **21**, 3655 (2011).

[12] T. Yokobori, M. Okawa, K. Konishi, R. Takei, K. Katayama, S. Oozono, T. Shinmura, T. Okuda, H. Wadati, E. Sakai, K. Ono, H. Kumigashira, M. Oshima, T. Sugiyama, E. Ikenaga, N. Hamada, and T. Saitoh, Phys. Rev. B **87**, 195124 (2013).

[13] J. J. Zhu, W. W. Li, G. S. Xu, K. Jiang, Z. G. Hu, M. Zhu, and J. H. Chu, Appl. Phys. Lett. **98**, 091913 (2011).

[14] G. E. Jellison Jr. and F. A. Modine, Appl. Phys. Lett. **69**, 371 (1996); **69**, 2137 (1996).

[15] M. J. Han, K. Jiang, J. Z. Zhang, Y. W. Li, Z. G. Hu, and J. H. Chu, Appl. Phys. Lett. **99**, 131104 (2011).

[16] J. Tauc, R. Gigorovici, and A. Vancu, Phys. Status Solidi **15**, 627 (1966).

[17] D. Li, X. D. Fang, Z. H. Deng, S. Zhou, R. H. Tao, W. W. Dong, T. Wang, Y. P. Zhao, G. Meng, and X. B. Zhu, J. Phys. D: Appl. Phys. **40**, 4910 (2007).

[18] R. Gillen and J. Robertson, Phys. Rev. B **84**, 035125 (2011).

[19] J. Bhosale, A. K. Ramdas, A. Burger, A. Muñoz, A. H. Romero, M. Cardona, R. Lauck, and R. K. Kremer, Phys. Rev. B **86**, 195208 (2012).

[20] J. Serrano, Ch. Schweitzer, C. T. Lin, K. Reimann, M. Cardona, and D. Fröhlich, Phys. Rev. B **65**, 125110 (2002).

[21] S. Levcenco, S. Doka, V. Tezlevan, D. Fuertes Marron, L. Kulyuk, T. Schedel-Niedrig, M. Ch. Lux-Steinerb, and E. Arushanov, Physica B **405**, 3547 (2010).

[22] J. D. Dow and D. Redfield, Phys. Rev. B **5**, 594 (1972).

[23] S. M. Wasim, G. Marn, C. Rincón, G. Sánchez Pérez, and A. E. Mora, J. Appl. Phys. **83**, 3318 (1998).

[24] H. Hiraga, T. Makino, T. Fukumura, A. Ohtomo, and M. Kawasaki, Appl. Phys. Lett. **95**, 211908 (2009).
[25] D. Shin, J. S. Foord, R. G. Egdell, and A. Walsh, J. Appl. Phys. **112**, 113718 (2012).
[26] H. Hiraga, T. Makino, T. Fukumura, H. Weng, and M. Kawasaki, Phys. Rev. B **84**, 041411 (2011).
[27] M. G. Brik, N. M. Avram, and C. N. Avram, Solid State Commun. **132**, 831 (2004).
[28] D. O. Scanlon, A. Walsh, B. J. Morgan, G. W. Watson, D. J. Payne, and R. G. Egdell, Phys. Rev. B **79**, 035101 (2009).
[29] D. S. McClure, J. Chem. Phys. **38**, 2289 (1963).
[30] A. F. Goncharov, V. V. Struzhkin, and S. D. Jacobsen, Science **312**, 1205 (2006).
[31] S. Lany, Phys. Rev. B **87**, 085112 (2013).
[32] E. Arca, K. Fleischer, S. A. Krasnikov, and I. Shvets, J. Phys. Chem. C **117**, 21901 (2013).
[33] F. Farzaneh and M. Najafi, J. Sci. Islamic Repub. Iran **22**, 329 (2011).
[34] D. W. Hamby, D. A. Lucca, M. J. Klopfstein, and G. Cantwell, J. Appl. Phys. **93**, 3214 (2003).
[35] J. L. Merz, H. Kukimoto, K. Nassau, and J. W. Shiever, Phys. Rev. B **6**, 545 (1972).
[36] N. A. M. Shanid and M. A. Khadar, Thin Solid Films **516**, 6245 (2008).
[37] M. Yin, C. K. Wu, Y. B. Lou, C. Burda, J. T. Koberstein, Y. M. Zhu, and S. O'Brien, J. Am. Chem. Soc. **127**, 9506 (2005).
[38] T. Ito and T. Masumi, J. Phys. Soc. Jpn. **66**, 2185 (1997).
[39] T. Okuda, N. Jufuku, S. Hidaka, and N. Terada, Phys. Rev. B **72**, 144403 (2005).
[40] C. S. Cheng, H. Gomi, and H. Sakata, Phys. Status Solidi A **155**, 417 (1996).
[41] P. Achatz, O. A. Williams, P. Bruno, D. M. Gruen, J. A. Garrido, and M. Stutzmann, Phys. Rev. B **74**, 155429 (2006).
[42] M. Y. Han, J. C. Brant, and P. Kim, Phys. Rev. Lett. **104**, 056801 (2010).
[43] H. Qiu, T. Xu, Z. L. Wang, W. Ren, H. Y. Nan, Z. H. Ni, Q. Chen, S. J. Yuan, F. Miao, F. Q. Song, G. Long, Y. Shi, L. T. Sun, J. L. Wang, and X. R. Wang, Nature Commun. **4**, 2642 (2013).